

# Optimization of Vibration and Noise Performance of Permanent Magnet Synchronous Motor for Electric Vehicles

LIU Huijuan\*, SONG Tengfei, ZHANG Zhenyang, DU Jinwen

School of Electrical Engineering, Beijing Jiaotong University, Beijing 100044, P. R. China

(Received 15 May 2019; revised 7 January 2020; accepted 15 January 2020)

**Abstract:** In the design of the motor used for electric vehicles (EVs), vibration and noise problems are often ignored, which reduce the reliability and service life of the motor. In this paper, an interior permanent magnet synchronous motor (IPMSM) with high power density is taken as an example, and its electromagnetic vibration and noise problem is investigated and optimized. Firstly, the factors that generate the electromagnetic force harmonic of IPMSM are analyzed by theoretical derivation. Furthermore, the mode and electromagnetic harmonic distribution of the motor are calculated and analyzed by establishing the electromagnetic-structure-sound coupling simulation model. Then, by combining finite element method (FEM) with modern optimization algorithm, an electromagnetic vibration and noise performance optimization method is proposed in the electromagnetic design stage of the motor. Finally, an IPMSM is optimized by this method for electromagnetic vibration and noise performance. The results of comparison between before and after optimization prove the feasibility of the method.

**Key words:** electric vehicle (EV); vibration and noise performance optimization; interior permanent magnet synchronous motor (IPMSM); finite element method (FEM)

**CLC number:** TM315      **Document code:** A      **Article ID:** 1005-1120(2020)02-0332-11

## 0 Introduction

Due to the increasing pollution of the environment, the new energy electric vehicle (EV) has gradually replaced fuel vehicles and has been widely used. As a key component of EV, the performance of electric motors directly determines the superiority of electric vehicles. Among all automotive motors, interior permanent magnet synchronous motor (IPMSM) dominates the market with its high power density and wide speed range<sup>[1-2]</sup>.

In previous studies, researchers mainly focused on the performance of motor, such as electromagnetic performance, temperature characteristics, or manufacturing cost. Therefore, power density<sup>[3]</sup>, price<sup>[4-5]</sup>, and temperature rise<sup>[6]</sup> are often defined as

design optimization objectives. A Pareto-based multi-objective differential evolution algorithm for EVs was used to design an in-wheel switched reluctance motor, in which torque per motor lamination volume, and efficiency were specified as objective functions<sup>[3]</sup>. In order to save computation time and study the thermal performance of the permanent magnet motor, the thermal network model combined with the finite element method (FEM) of the totally enclosed water-cooled permanent magnet machine was established<sup>[4]</sup>. In addition, the price also determines the competitiveness of the motor. Ref. [6] used magnetic equivalent circuit and  $k$ -means clustering algorithm to acquire the best efficiency per weight and cost of the IPMSM.

However, the vibration and noise performance

\*Corresponding author, E-mail address: hjliu@bjtu.edu.cn.

**How to cite this article:** LIU Huijuan, SONG Tengfei, ZHANG Zhenyang, et al. Optimization of vibration and noise performance of permanent magnet synchronous motor for electric vehicles[J]. Transactions of Nanjing University of Aeronautics and Astronautics, 2020, 37(2): 332-342.

<http://dx.doi.org/10.16356/j.1005-1120.2020.02.014>

of the motor was often neglected while improving the electromagnetic-thermal performance. This inevitably makes the vibration and noise performance of the motor worse. Excessive vibration will reduce the reliability and service life of the motor components<sup>[7]</sup>, and excessive noise will reduce the comfort during driving. Therefore, vibration and noise are also important factors to be considered and studied in the design process.

In the existing research on vibration and noise of motor, it mainly includes numerical calculation methods, measurement methods, power modulation methods, etc.

In terms of numerical calculation, Ref.[8] mainly described how to accurately calculate the noise problem by using multi-physical coupling fields, including the influence of tangential force and damping ratio on noise calculation. Ref.[9] also provided a calculation flowchart of the multi-physics model for vibration and noise of an external-rotor axial-flux motor and experiments were carried out to verify its accuracy. In addition, a lot of studies on the vibration and noise of permanent magnet synchronous motors are carried out with variable speeds, including noise prediction, sound quality analysis<sup>[10]</sup> and current harmonics<sup>[11]</sup>.

The modulation mode of the power supply also has a greater impact on the electromagnetic force and vibration of the motor<sup>[12-13]</sup>. The influence of spatial mode, armature winding frequencies, the carrier frequency on the vibration noise of a PMSM was studied in Ref.[12] and it was found that new harmonic components would be introduced into the vibration spectrum of the motor by using PWM modulation method. Ref.[13] investigated vibration and noise under different supply currents and also found that the current harmonics from PWM induced extra vibration and noise frequencies and increased the sharpness of noise due to their high frequency.

In terms of noise testing and diagnosis, a novel black and white box method is proposed to diagnose

and optimize the abnormal noise and vibration of the PMSM<sup>[14]</sup>. In Ref.[15], modulation effect of slotted structure on vibration and noise was studied. It is found that high-order space electromagnetic force may also cause low-order large-amplitude electromagnetic vibration. Moreover, the electromagnetic and vibration noise performance of IPMSM, switched reluctance motor and induction motor used for EVs were compared in Ref.[16]. Ref.[17] presented the effect of rotor eccentricity and glue of permanent magnet (PM) on vibration and noise, also emphasized the importance of damping ratios for simulation and experiment.

In the references above, the problem of motor vibration and noise is often simply calculated or experimentally verified, whereas, few studies have suggested how to optimize the vibration and noise performance in the design process of the motor. How to optimize the vibration and noise performance from the perspective of motor design is also rarely proposed. Plus, the structure-sound field model requires large memory and computational expense. It is impractical to optimize the vibration noise in these two fields. Therefore, it is very important to find an appropriate vibration and noise optimization method.

In this paper, the vibration and noise performance of a 70 kW IPMSM is studied and optimized. Firstly, the spatial and temporal component of electromagnetic force harmonics is theoretically derived, which is the main cause of motor vibration and noise. Secondly, in order to verify the accuracy of theoretical analysis, electromagnetic FEM and structural-sound field coupling model are established to calculate the electromagnetic force harmonic component and sound pressure level (SPL) of the motor. Finally, by combining modern optimization algorithms with FEM, a method for optimizing vibration and noise performance of motor in an electromagnetic field is proposed, and the vibration and noise performance of motor is compared.

## 1 Theoretical Analysis on Electromagnetic Force

The harmonic of the radial electromagnetic force acting on the stator teeth is the main cause of the electromagnetic vibration and noise of IPMSM<sup>[10]</sup>. When the temporal frequency and the spatial order of electromagnetic force coincide with the natural mode of the motor, the motor resonates, which in turn generates large vibration and noise. In this section, the spatial and temporal characteristics of the electromagnetic force of IPMSM are theoretically analyzed.

According to the Maxwell tensor method, the radial force density  $P_r$  on the stator tooth is

$$P_r(\theta, t) = \frac{1}{2\mu_0} [b_r^2(\theta, t) - b_t^2(\theta, t)] \approx \frac{b_r^2(\theta, t)}{2\mu_0} \quad (1)$$

where  $b_r(\theta, t)$  is the radial components of flux density in the air gap,  $b_t(\theta, t)$  the tangential components of flux density in the air gap, and  $\mu_0$  the vacuum permeability. Radial component of flux density  $b_r(\theta, t)$  is the main factor, so tangential magnetic density  $b_t(\theta, t)$  is ignored.

The radial flux density  $b_r(\theta, t)$  can be written as

$$b_r(\theta, t) = f(\theta, t) \cdot \Lambda_g(\theta, t) = [f_{\text{arm}}(\theta, t) + f_{\text{mag}}(\theta, t)] \cdot \Lambda_g(\theta, t) \quad (2)$$

where  $f(\theta, t)$  is the magnetomotive force (MMF) in the air gap,  $\Lambda_g(\theta, t)$  the air gap permeance,  $f_{\text{arm}}(\theta, t)$  the MMF caused by armature reaction field,  $f_{\text{mag}}(\theta, t)$  the MMF caused by PM field, and  $\theta$  the mechanical angular position.

The air gap permeance  $\Lambda_g(\theta, t)$  can be written as

$$\Lambda_g(\theta, t) = \sum_{k_1=0,1,2,\dots}^{\infty} \Lambda_{k_1} \cos(k_1 z_1 \theta) \quad (3)$$

where  $\Lambda_{k_1}$  is the magnitude of the  $k_1$ th harmonic permeance and  $z_1$  the number of stator slot.

The MMF  $f_{\text{arm}}(\theta, t)$  caused by armature reaction field and MMF  $f_{\text{mag}}(\theta, t)$  caused by PM field can be written as

$$f_{\text{arm}}(\theta, t) = \sum_v^{\infty} F_v \cos(vp\theta - \omega_1 t) \quad (4)$$

$$f_{\text{mag}}(\theta, t) = \sum_u^{\infty} F_u \cos(up\theta - u\omega_1 t - \varphi_u) \quad (5)$$

where  $v=6k_2+1, k_2=\pm 1, \pm 2, \dots, u=2k_3+1, k_3=\pm 1, \pm 2, \dots, p$  is the number of pole-pairs,  $\omega_1$  the angular frequency of fundamental magnetic potential,  $F_v$  the magnitude of the  $v$ th MMF caused by armature reaction field,  $F_u$  the magnitude of the  $u$ th harmonic MMF caused by PM field, and  $\varphi_u$  the phase angle of the  $u$ th harmonic MMF caused by PM field.

Substituting Eqs.(3)–(5) into Eq.(2), radial components of flux density  $b_r(\theta, t)$  can be obtained

$$b_r(\theta, t) = \sum_v^{\infty} \sum_{k_1}^{\infty} \frac{F_v \Lambda_{k_1}}{2} \cos[(vp \pm k_1 z_1)\theta - \omega_1 t] + \sum_u^{\infty} \sum_{k_1}^{\infty} \frac{F_u \Lambda_{k_1}}{2} \cos[(up \pm k_1 z_1)\theta - u\omega_1 t - \varphi_u] = b_{r,\text{arm}}(\theta, t) + b_{r,\text{mag}}(\theta, t) \quad (6)$$

where  $b_{r,\text{arm}}(\theta, t)$  is the flux density caused by armature reaction field, and  $b_{r,\text{mag}}(\theta, t)$  the flux density caused by PM field. Therefore, the radial force density  $P_r$  on the stator tooth can be obtained

$$P_r(\theta, t) = \frac{1}{2\mu_0} [b_{r,\text{arm}}^2(\theta, t) + 2b_{r,\text{arm}}(\theta, t)b_{r,\text{mag}}(\theta, t) + b_{r,\text{mag}}^2(\theta, t)] \quad (7)$$

It can be seen that the air gap electromagnetic radial force density can be divided into three parts: The first part is produced by the interaction of armature reaction field; the second part is produced by the interaction of PM field; and the third part is produced by the interaction of armature reaction field and PM field. Therefore, the spatial order and frequency of radial force density from these three parts can be achieved, as shown in Table 1.

In addition, the relationship between deformation  $\Delta d$  of stator (equivalent to a cylinder) and spatial mode order  $r$  is approximately expressed as

$$\Delta d \propto \frac{1}{r^4} \quad (8)$$

It can be known that the higher the spatial order is, the smaller the amplitude of the vibration

**Table 1 Spatial order and frequency of radial force density**

Source	Spatial order	Frequency
Interaction of PM field	$(u_1 \pm u_2)p + k_1 z_1$	$(u_1 \pm u_2)f$
Interaction of armature reaction field	$(v_1 \pm v_2)p + k_1 z_1$	$2f, 0$
Interaction of armature reaction and PM field	$(v \pm u)p + k_1 z_1$	$(u_1 \pm 1)f$

generated by the electromagnetic force will be. Therefore, we should pay more attention to the electromagnetic harmonics force with lower spatial order and ignore high spatial order harmonics in the vibration and noise analysis.

## 2 Multi-physical Field Coupling Calculation

In order to study the spatial and temporal characteristics of electromagnetic force harmonics and vibration noise, the 2D-FEM of electromagnetic field and the structural-acoustic coupled field model are established in this section. The electromagnetic force harmonics calculated by the electromagnetic FEM are input into the structure-sound coupling field as the input source.

### 2.1 FEM of electromagnetic field

In this paper, an 8-pole 48-slot IPMSM is taken as an example, and its vibration, noise and electromagnetic characteristics are studied, as shown in Fig.1. It can be seen that in order to save the computational cost, the 1/8 2D-FEM is established, which contains 24 515 nodes and 5 489 elements. The main parameters of motor are given in Table 2. Because the vibration noise during the peak condition of the motor, that is, during the acceleration of the electric vehicles, is more obvious, this section mainly analyzes the electromagnetic force under the peak working condition.

Fig.2(a) shows the temporal-spatial distribution of the air gap magnetic density in one pair of poles and an electrical cycle, where the abscissa represents the temporal period and the ordinate repre-

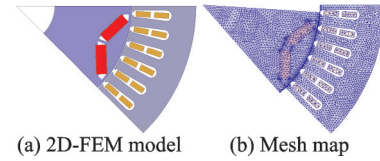


Fig.1 2D-FEM and mesh map diagram

**Table 2 Main performance parameters of motor**

Parameter	Value	Parameter	Value
Pole	8	Slot	48
Max current/ A	200	Max voltage/ V	220
Rated speed/ (r•min <sup>-1</sup> )	3 000	Rated torque/ (N•m)	90
Rated power/ kW	30	Peak power/ kW	60
Max torque/ (N•m)	220	Max speed/ (r•min <sup>-1</sup> )	9 000

sents the spatial period. It can be seen that the air gap magnetic density is sinusoidal in appearance from the temporal angle or spatial angle. Fig.2(b) shows its temporal-spatial 2D-FFT results. It can be seen that in addition to the fundamental wave  $(1p, 1f_1)$ , the air gap magnetic density contains a large harmonic content, and these harmonics are caused by the tooth structure, winding distribution, and air gap permeability.

It also can be seen that air gap magnetic density is distributed periodically in both spatial and temporal angles. From 2D-FFT decomposition, and the spatial order and temporal frequency of larger harmonic contents are mainly  $(2k+1)p$  ( $k=0, 1, 2, \dots$ ) or  $(2k+1)f_1$ . Meanwhile, except for the fundamental magnetic field  $(p, f)$ , the harmonic magnetic fields with orders  $(5p, 5f)$ ,  $(12p, -1f)$ ,  $(7p, 7f)$  are also relatively large. This is mainly because the spatial order of tooth harmonic in the magnetic field is  $(2mk \pm 1)p$  ( $m$  is the number of phases), which is too large and cannot be reduced by using the distributed winding and other methods. Therefore, tooth harmonic is the main cause of electromagnetic vibration noise of motor.

Similarly, the temporal-spatial distribution and 2D-FFT decomposition of air gap electromagnetic force density under peak load can also be obtained

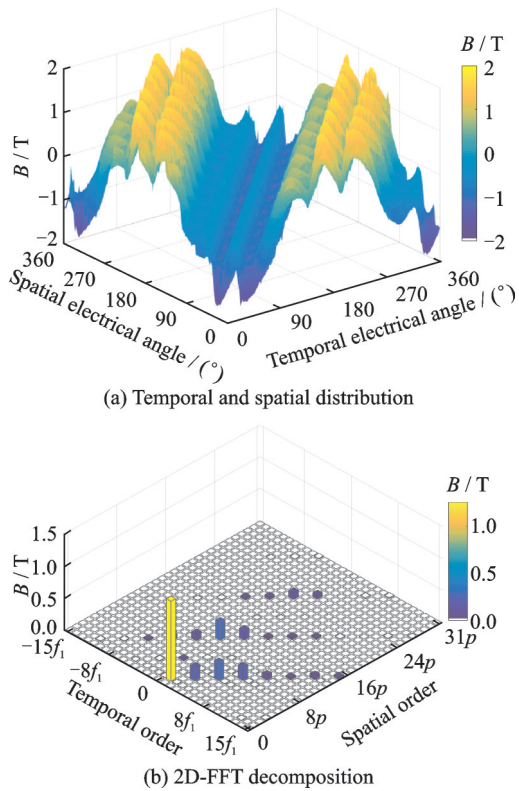


Fig.2 Temporal and spatial distribution and 2D-FFT decomposition of air gap magnetic density

by Maxwell tensor method and Eq. (1). Here, Fig.3(a) shows the temporal-spatial distribution of the air gap radial force density in a pair of poles and an electrical cycle. Fig.3(b) shows the temporal-spatial 2D-FFT results, where the abscissa represents the temporal order (unit is  $f_1$ ) and the ordinate represents the spatial order (unit is  $p$ ).

From Fig.3(b), it can be seen that the spatial orders of larger harmonic contents are mainly  $2kp$  ( $k=0, 1, 2, \dots$ ) and the same as temporal order. That is to say, the air gap electromagnetic force harmonic of the IPMSM with integer slot only contains the even harmonic. Simultaneously, the 2D-FFT decomposition results are basically consistent with the theoretical analysis results, as shown in Table 1, which verifies the accuracy of the theoretical analysis. According to Eq. (8), it can be known that electromagnetic harmonics force with lower spatial can cause a larger vibration and noise. Combined with Fig.3, the electromagnetic harmonic forces with lower spatial order (0 or  $2p$ ) deserve more atten-

tion.

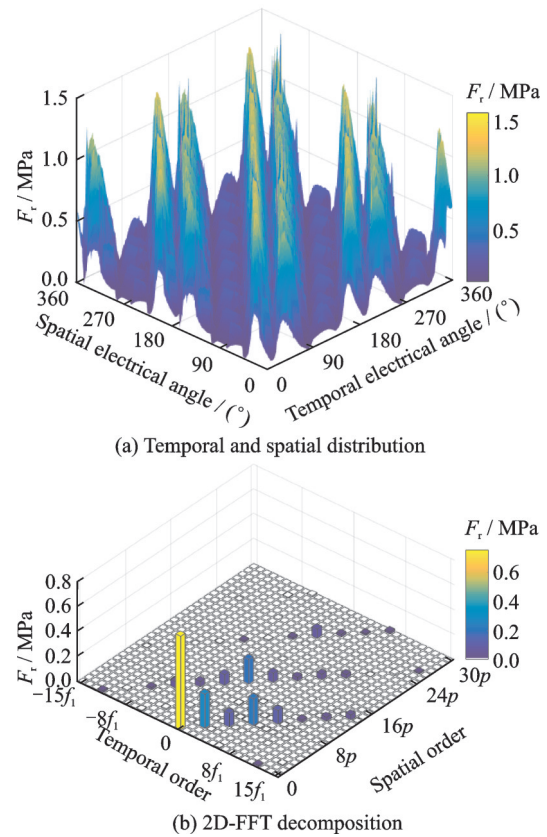


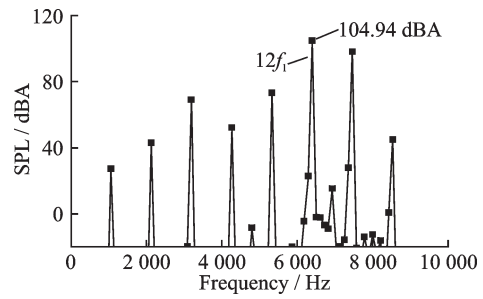
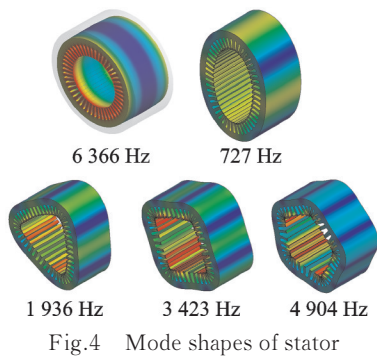
Fig.3 Temporal and spatial distribution and 2D-FFT decomposition of air gap force density

## 2.2 Structural-acoustic coupling field calculation

According to the oscillation equation, the motor will have a larger resonance when the natural frequency of the mode and the frequency of the electromagnetic force coincide with each other. Therefore, it is necessary to analyze the natural mode of the stator firstly.

By structural field model, mode results of the stator from simulation are obtained, as is shown in Fig.4. The calculation results of modes 0 to 5 are 6 366, 727, 1 936, 3 423 and 4 904 Hz. Among them, 0-order mode is a very important factor in the analysis of vibration and noise. And other modes with higher spatial order have little effect on vibration and noise, so they are not considered.

By establishing the structural-sound coupling field model, the noise spectrum and distribution of



the motor can be obtained. Fig.5 shows the SPL distribution of the motor under peak load within 1 m. It can be seen that the sound is distributed in an umbrella shape in the air. And the closer to the motor, the louder the noise is.

trated in the high-speed area and the 0-order mode. There are two main reasons: When the IPMSM is in high speed condition, the air gap harmonic caused by flux weakening increases; and the  $12f_1$  harmonic caused by the tooth harmonic, which can be not reduced, is now close to the 0-order mode.

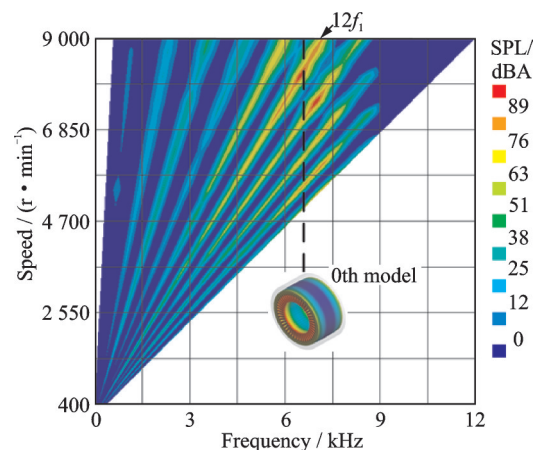
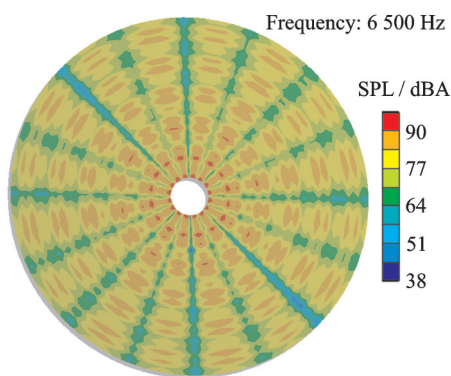


Fig.5 SPL distribution within 1 m of motor

Fig.7 SPL waterfall map of noise spectrum

In addition, it can also obtain the noise spectrum of the motor under a certain working condition. Fig.6 shows the noise spectrum of a point 1 m away from the motor when the motor is running at a certain speed ( $8\ 000\ \text{r}\cdot\text{min}^{-1}$ ,  $83\ \text{N}\cdot\text{m}$ ,  $f_1=533.33\ \text{Hz}$ ). According to Fig.3(b), the temporal orders of electromagnetic force are  $2f_1, 4f_1, \dots, 12f_1$ , which all cause the noise of the motor. In these components, the frequency of the  $12f_1$  harmonic force coincides with the 0-order mode of stator in this load condition. Therefore, a large noise is generated, which is 104.94 dBA.

It can also obtain the noise spectrum of the motor under full speed range. Fig.7 shows the waterfall map of noise spectrum of the motor at full speed range. The areas with high noise are mainly concen-

### 3 Optimization

#### 3.1 Optimization design flow

Although the vibration and noise of the motor can be calculated in the structural-acoustic coupling field, the computational cost and calculation time required for calculation are very large. Therefore, it is difficult to optimize the vibration and noise of the motor in the coupled field.

Based on the above research, we can know that electromagnetic force harmonics, especially tooth harmonics (the 6th and the 12th harmonics), are the main cause of motor vibration and noise. Therefore, the problem of optimizing the electro-

magnetic vibration noise can be transformed into the problem of optimizing the electromagnetic force harmonic, thereby greatly reducing the computational cost and time.

Fig.8 shows the specific flow chart of the proposed optimization method. The optimization method mainly includes two aspects.

The first step is to optimize the electromagnetic performance of the motor by the sensitivity analysis, FEM and MPSO methods. At this time, the optimization objectives are the weight, price, and power density of the motor. The optimization variables are stator outer and diameter, length and slot depth, and PM size. The specific process of the electromagnetic optimization method has been mentioned in the previous study<sup>[5]</sup>, and will not be described in detail here. The flowchart of optimization process of the MPSO algorithm is shown in Fig.9.

The variables, objective functions and constraints in the design process are illustrated above, so the multi-objective optimization problem of PM drive motor can be expressed as

$$\begin{aligned} \min & F_{\text{obj}}(x) \\ \text{s.t.} & g(x) \leq 0 \\ & x_{i, \min} \leq x \leq x_{i, \max} \\ & x_i \in X, i = 1, 2, \dots, D \end{aligned} \quad (9)$$

where  $g(x)$  is the constraint,  $x$  the variables, and  $F_{\text{obj}}$  the optimization objective function.

When the optimized motor performance meets the requirements, the optimization of the vibration and noise performance will continue in the electromagnetic field. The tooth harmonic in the electromagnetic force is taken as the optimization objective, which are the 6th and the 12th harmonics. The optimization variables are PM arrangement, angle and auxiliary slot form, which basically do not affect the power density and the price of the motor.

By electromagnetic and MSPO, the 6th and the 12th harmonics will be optimized. As shown in Fig.10, the Pareto Front is used to determine the

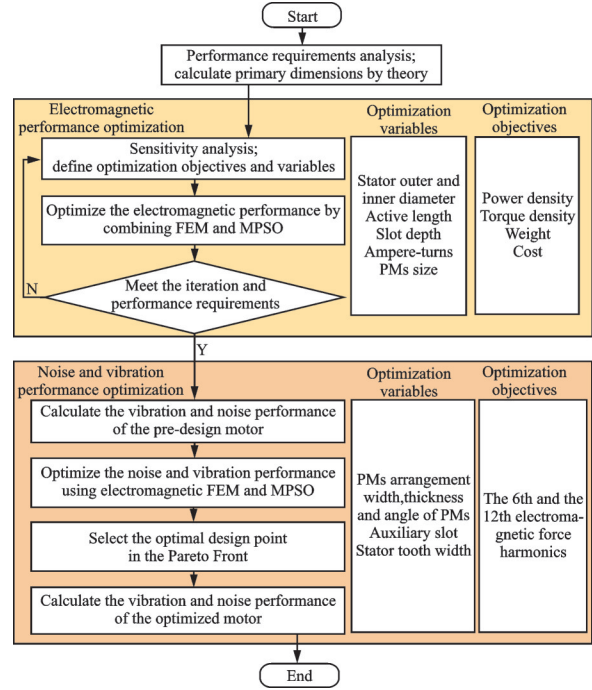


Fig.8 Flowchart of optimization procedure

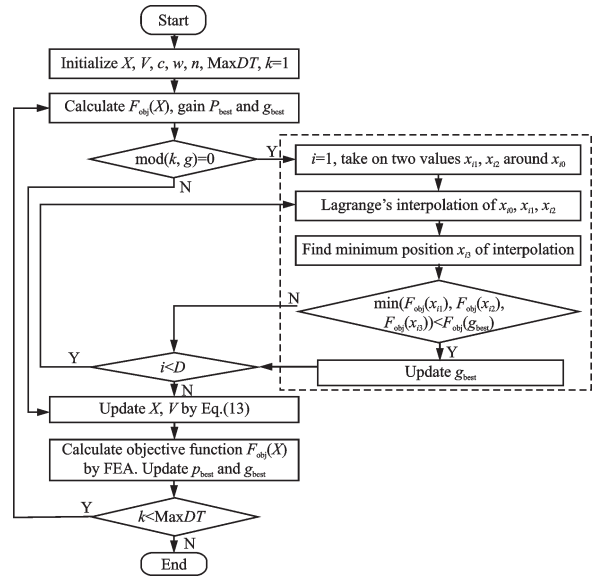


Fig.9 Flowchart of MPSO algorithm

optimal value in the multi-objective optimization process. Through multiple iterations, the population gradually tends to the optimal position, and we can select the optimal solution from the Pareto Front. After selecting the optimal point, the optimized vibration and noise performance of the motor is calculated through the structural acoustic coupling field to judge the feasibility of the optimization method.

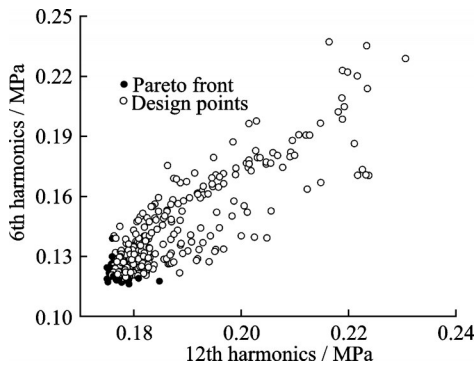


Fig.10 Pareto front of the optimal solutions

### 3.2 Comparison before and after optimization

The comparison of rotor topology before and after optimization is shown in Fig.11. It can be seen that in order to modulate a better air gap magnetic density waveform, the angle of the PM also changes and the rotor structure is optimized from V-type PM to V1-type PM (the total amount weight of PM has not changed). Besides, two auxiliary grooves are made in the outer circle of the rotor.

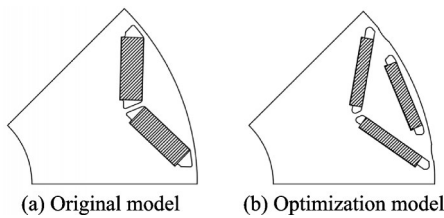


Fig.11 Comparison of optimization and original model

Firstly, we observe the changes in the electromagnetic properties of the motor. Fig.12 shows the comparison of the cogging torque and peak torque. It can be seen that the cogging torque and torque ripple are also greatly reduced while the root mean square (RMS) of peak torque is not excessively reduced. This is good for the transmission of torque and reduction of the noise. Therefore, the electromagnetic performance of the motor is guaranteed while the noise performance of the motor is optimized.

Fig.13 shows the comparison of temporal FFT decomposition of the 0-order spatial force density before and after optimization. Through optimization, the 6th time harmonic  $6f_1$  and the 12th time harmonic  $12f_1$  of the 0-order spatial electromagnetic force

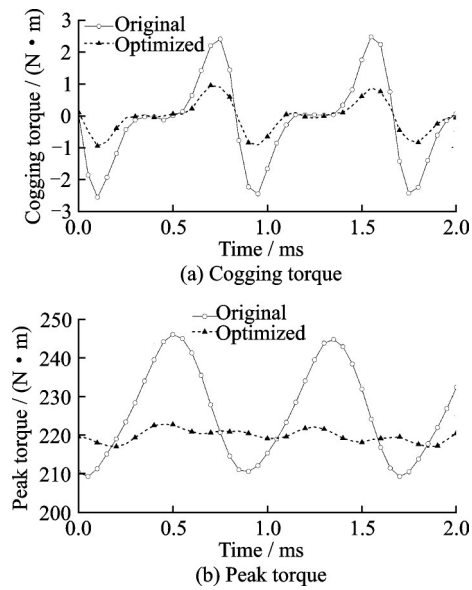


Fig.12 Comparison of cogging and peak torque

density, which have great influence on vibration and noise, are greatly reduced. Similarly, the noise spectrum variation of the motor at high speed ( $8000 \text{ r}\cdot\text{min}^{-1}$ ) can also be obtained in an electromagnetic-structure-acoustic coupling field, as shown in Fig. 14. The noise maximum is reduced from 104.94 dBA to 96.06 dBA, with a total reduction of 7 dBA, which proves the effectiveness of this optimization method.

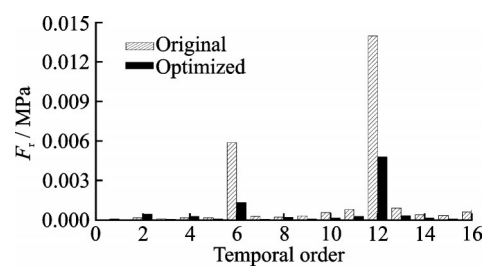


Fig.13 Comparison of temporal FFT decomposition of the 0-order spatial air gap force density

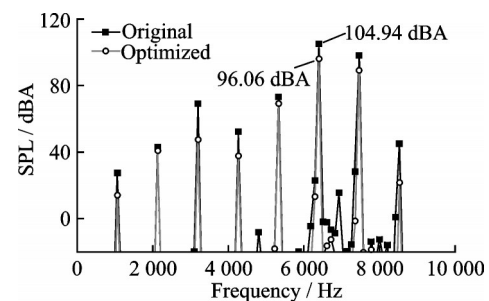


Fig.14 Comparison of noise spectrum of motor at  $8000 \text{ r}\cdot\text{min}^{-1}$

The specific performance values before and after optimization are shown in Table 3. It can be seen that through optimization, not only the cogging torque and torque ripper of the motor are optimized, but also the max SPL of the motor is greatly reduced. However, the maximum power and maximum torque are slightly reduced. This is because the arrangement and size of the permanent magnets have been adjusted for better air gap magnetic density. This inevitably causes a slight drop in the amplitude of magnetic density, resulting in a reduction in the maximum torque. But this tiny reduction can be tolerated. The optimization method proposed in this paper starts with the theoretical analysis of electromagnetic force harmonics of IPMSM, that is, the essential causes of motor noise and vibration, and then optimizes it with multi-objective optimization to achieve noise reduction.

**Table 3 Comparison between original and optimized motor**

Parameter	Original	Optimized
Cogging torque/ (N·m)	5.03	1.90
Max torque/ (N·m)	225.4	219.7
Torque ripper/%	16.3	2.7
Max power/ kW	70.8	69.0
Max SPL/ dBA	104.94	96.06

In order to verify the effectiveness of the proposed optimization method, the experimental verification of the prototype is indispensable. However, the prototype has not been produced yet. In the next research, the prototype before and after optimization will be manufactured. Firstly, modal tests of the stator and shell assembly will be carried out, including testing the frequencies and damping ratios of different modal orders. And their electromagnetic performances, such as no-load back EMF, power-speed and torque-speed characteristic curves, will be tested and compared. Secondly, the acceleration of the shell surface under different working conditions will be obtained by the acceleration sensor. Fi-

nally, the SPL at 1 m away from the motor will also be tested and its spectral characteristics will be analyzed by Fourier decomposition.

## 4 Conclusions

This paper mainly proposes a vibration and noise analysis and optimization method of IPMSM. According to the Maxwell tensor method, the spatial and temporal characteristics of the air gap electromagnetic force are firstly derived theoretically. Then the correctness of the theoretical derivation is verified by establishing the electromagnetic FEM and calculation. It is found that the air gap electromagnetic force harmonic of the IPMSM with integer slot mainly contains the even harmonic, meanwhile, the harmonic force with spatial order 0 and  $2p$  deserves more attention.

Then, a structure-sound field coupling model is established, and the noise spectrum and distribution of the motor are obtained. It can be found that the area with large noise is mainly concentrated in the high-speed area, where the 12th harmonic of electromagnetic force coincides with the 0-order mode of the motor.

Finally, the multi-objective optimization method combining MPSO with FEM is used to optimize the 6th and the 12th harmonics of the electromagnetic force. Through optimization, the maximum SPL of the motor is reduced from 104.94 dBA to 96.06 dBA while the electromagnetic performance of the motor, such as torque ripple, is also improved and power density has not obviously decreased. The feasibility and effectiveness of the optimization method are verified.

In the future study, to verify the accuracy and effectiveness of the proposed method, we will carry out modal testing of the stator assembly to verify and correct the accuracy of modal simulation. And the experiment bench will be built for the electromagnetic performance and vibration and noise test of prototypes before and after optimization.

## References

- [1] WEIDUO Z, XUEJIAO W, CHRIS G. Multi-physics and multi-objective optimization of a high speed pmsm for high performance applications[J]. *IEEE Transactions on Magnetic*, 2018, 54(11): 1-5.
- [2] AHN K, BAYRAK A, PAPALAMBROS P. Electric vehicle design optimization: Integration of a high-fidelity interior-permanent-magnet motor model[J]. *IEEE Transactions on Vehicular Technology*, 2015, 64(9): 3870-3877.
- [3] OKSUZTEP E, EYYU P. In-wheel switched reluctance motor design for electric vehicles by using pareto based multi objective differential evolution algorithm[J]. *IEEE Transactions on Vehicular Technology*, 2016, 66(6): 4706-4715.
- [4] REZA I, YOUSEF A, HAMID Y. Techno-economic design optimization of an interior permanent-magnet synchronous motor by the multi-objective approach[J]. *IET Electric Power Applications*, 2018, 12(7): 972-978.
- [5] SONG T, ZHANG Z, LIU H, et al. Multi-objective optimization design and performance comparison of permanent magnet synchronous motor for EVs based on FEA[J]. *IET Electric Power Applications*, 2019, 13(8): 1157-1166.
- [6] ZHANG B, QU R, WANG J, et al. Thermal model of totally enclosed water-cooled permanent-magnet synchronous machines for electric vehicle application[J]. *IEEE Transactions on Industry Applications*, 2015, 51(4): 3020-3029.
- [7] FOK D, FRANSES P H, PAAP R. Vibroacoustic behaviour analysis of a permanent magnet synchronous machine for automotive applications[C]//*Proceedings of the 49th International Universities Power Engineering Conference (UPEC)*. Cluj-Napoca, Romania: IEEE, 2014.
- [8] TORREGROSSA D, PEYRAUT F, FAHIMI B, et al. Multiphysics finite-element modeling for vibration and acoustic analysis of permanent magnet synchronous machine[J]. *IEEE Transactions on Energy Conversion*, 2011, 26(2): 490-500.
- [9] DENG W, ZUO S. Axial force and vibroacoustic analysis of external-rotor axial-flux motors[J]. *IEEE Transactions on Industrial Electronics*, 2017, 65(3): 2018-2030.
- [10] LIN F, ZUO S, DENG W, et al. Modeling and analysis of electromagnetic force, vibration and noise in permanent magnet synchronous motor considering current harmonics[J]. *IEEE Transactions on Industrial Electronics*, 2016, 63(12): 7455-7466.
- [11] LIN F, ZUO S, DENG W, et al. Noise prediction and sound quality analysis of variable-speed permanent magnet synchronous motor[J]. *IEEE Transactions on Energy Conversion*, 2017, 32(2): 698-706.
- [12] TAKAFUMI H, TOSHIYUKI A, YOSUKE T, et al. Analysis of vibration and noise in permanent magnet synchronous motors with distributed winding for the PWM method[J]. *IEEE Transactions on Industry Applications*, 2018, 54(6): 6042-6049.
- [13] LIN F, ZUO S, DENG W, et al. Modeling and analysis of electromagnetic force, vibration, and noise in permanent-magnet synchronous motor considering current harmonics[J]. *IEEE Transactions on Industry Electronics*, 2016, 63(12): 7455-7466.
- [14] MA C, LIU Q, WANG D, et al. A novel black and white box method for diagnosis and reduction of abnormal noise of hub permanent magnet synchronous motors for electric vehicles[J]. *IEEE Transactions on Industrial Electronics*, 2016, 63(2): 1153-1167.
- [15] HAIYANG F, DAWEI L, RONGHAI Q, et al. Modulation effect of slotted structure on vibration response in electrical machines[J]. *IEEE Transactions on Industrial Electronics*, 2019, 66(4): 2998-3007.
- [16] YANG Z, SHANG F, MEMBER S, et al. Comparative study of interior permanent magnet, induction, and switched reluctance motor drives for EV and HEV applications[J]. *IEEE Transactions on Transportation Electrification*, 2017, 1(3): 245-254.
- [17] HE G, HUANG Z, QIN R, et al. Numerical prediction of electromagnetic vibration and noise of permanent-magnet direct current commutator motors with rotor eccentricities and glue effects[J]. *IEEE Transactions on Magnetics*, 2012, 48(5): 1924-1931.

**Acknowledgement** This work was supported by the Fundamental Research Funds for the Central Universities (No. 2019YJS181).

**Author** Prof. LIU Huijuan received Ph.D. in Electrical Engineering from Beijing Jiaotong University in 2009 and re-

ceived the B.S. degree and M.S. degree from Tianjin University in 1989 and 1994, respectively. She worked as a visiting scholar in the Laboratory for Power Electronics & Electrical Machines, The Ohio State University, Columbus, OH, USA, in 2008. In 2011 and 2013, She worked as a research fellow in The Hong Kong Polytechnic University. Since December 2015, she has been a professor in Beijing Jiaotong University. Her current research interests focus on numerical methods of electromagnetic field computation, optimal design and control of high performance electrical machines and novel electrical motors, such as induction machine, doubly

fed brushless machine, and permanent magnetic machine for wind power and other new power source development.

**Author contributions** Prof. LIU Huijuan contributed to the study, theoretical analysis of the model and prepared the manuscript. Mr. SONG Tengfei and Mr. DU Jinwen contributed finite element modeling and analysis. Mr. ZHANG Zhenyang contributed to the discussion and background of the study. All authors commented on the manuscript draft and approved the submission.

**Competing interests** The authors declare no competing interests.

(Production Editor: SUN Jing)

## 电动汽车用永磁同步电机电磁振动与噪声性能优化

刘慧娟, 宋腾飞, 张振洋, 杜晋文

(北京交通大学电气工程学院, 北京 100044, 中国)

**摘要:**在以往的电动汽车驱动电机设计中,经常忽略电机的电磁振动噪声问题,这无疑会降低车用电机的运行可靠性和使用寿命。为此,本文以一台车用内置式永磁同步电机为例,提出了一种在驱动电机电磁设计时进行电磁振动噪声分析和优化的方法。首先,基于电磁场理论和麦克斯韦应力张量法,推导并分析了引起电机电磁振动噪声的主要因素——气隙电磁力的主要空间和时间谐波构成。其次,通过建立电机电磁-结构-声多物理场耦合仿真模型,仿真分析了电机气隙径向电磁力时空谐波分布和定子模态分布,并初步计算了电机在高速工况下的振动和噪声性能。然后,结合有限元分析和现代优化算法,提出了一种在电磁设计阶段进行驱动电机电磁振动和噪声性能的优化方法。最后,通过所提出的电磁振动噪声优化方法改善了一台内置式永磁同步电机的电磁振动和噪声性能,并通过对比优化前后电机的电磁振动噪声性能,验证了所提出优化方法的可行性和有效性。

**关键词:**电动汽车;振动与噪声优化;内置式永磁同步电机;有限元方法